CORE
Metadata, citation and similar papers at core.ac.uk
Provided by Universidade do Minho: RepositoriUM

DESIGN FORMULA TO EVALUATE THE NSM FRP STRIPS SHEAR STRENGTH CONTRIBUTION TO A RC BEAM

Vincenzo Bianco [1], Giorgio Monti [2] and J.A.O. Barros [3]

Abstract:

This paper presents the closing step of a synthesis process aiming at deriving, from a previously developed more complex model, a simple design formula to evaluate the shear strength contribution provided by a system of Near Surface Mounted (NSM) Fiber Reinforced Polymer (FRP) strips to a Reinforced Concrete (RC) beam. The self-contained and ready-to-implement set of analytical equations and logical operations is presented along with the main underlying physical-mechanical principles and assumptions. The formulation proposed is appraised against some of the most recent experimental results and its predictions are also compared with those obtained by the two previous and more sophisticated versions of the same modeling strategy. Monte Carlo simulations are carried out in order to appraise the sensitivity of the NSM shear strength contribution prediction to the value assumed by the input parameters.

Keywords: Shear; Strengthening; FRP; C. Analytical modeling; Monte Carlo simulations.

Introduction

Shear strengthening of RC beams by NSM technique consists of gluing FRP strips by a structural adhesive into thin shallow slits cut onto the concrete cover of the beam web lateral faces. A comprehensive three-dimensional mechanical model to predict the NSM FRP strips shear strength contribution to a RC beam was recently proposed (Bianco 2008, Bianco *et al.* 2009a-b and 2010). That model was developed fulfilling equilibrium, kinematic compatibility and constitutive laws of both the materials involved (FRP and concrete), as well as the local bond between themselves. Despite its consistency with experimental recordings, that model turned out to be somehow cumbersome to be easily implemented and accepted by professional structural engineers. More recently, a simpler version of that model was derived from the more complex one by introducing the following simplifications (Bianco 2008, Bianco *et al.* 2011): 1) a bi-linear rigid-softening local bond stress-slip diagram was adopted instead

[1] Post Doctoral Reseracher, Dept. of Structural Engrg. and Geotechnics, Sapienza University of Rome, via A. Gramsci 53, 00197 Rome, taly. E-mail: vincenzo.bianco@uniroma1.it, corresponding Author. Tel. +39 0649919254, Fax. +39 063221449.
[2] Full Professor, Dept. of Structural Engrg. and Geotechnics, Sapienza University of Rome, via A. Gramsci 53, 00197 Rome, Italy. E-mail: giorgio.monti@uniroma1.it.
[3] Full Professor, Dept. of Civil Engineering, University of Minho, Campus de Azurém, 4810-058 Guimarães, Portugal. E-mail: barros@civil.uminho.pt .

of a multilinear diagram, 2) concrete fracture surface was assumed as semi-pyramidal instead of semi-conical, 3) attention was focused on the average-available-bond-length NSM FRP strip glued on the relevant prism of surrounding concrete, 4) determining the constitutive law of the average-available-bond-length NSM strip, along the approach followed for Externally Bonded Reinforcement (EBR) by Monti *et al.* (2003), and 5) determining the maximum effective capacity attainable by the average-available-bond-length NSM strip bridging the shear failure crack, imposing a coherent kinematic mechanism (*e.g.* Monti *et al.* 2004, Monti and Liotta 2007). Nevertheless, even the second version of that model resulted not easy enough to be accepted by structural engineers since, in order to obtain the constitutive law of the average-available-bond-length NSM strip, it is necessary to implement an iterative procedure simulating the increasing value of the imposed end slip.

In the present paper, the main physical features of a more simplified version of that mechanical model are presented along with the further simplifications introduced with respect to the former version.

During the loading process of a RC beam subject to shear, when concrete average tensile strength f_{ctm} is attained at the web intrados (Fig. 1), some shear cracks originate therein and successively progress towards the web extrados. The governing shear failure crack, herein designated as Critical Diagonal Crack (CDC), is inclined of an angle θ with respect to the beam longitudinal axis (Fig. 1a). The CDC can be schematized as an inclined plane dividing the web into two portions sewn together by the crossing strips (Fig. 1a). At load step t_1, the two web parts, separated by the CDC, start moving apart by pivoting around the crack tip whose trace, on the web face, is point *E* in Fig. 1a. From that step on, by increasing the applied load, the CDC opening angle $\gamma(t_n)$ progressively widens (Fig. 1a). The strips crossing the CDC oppose its widening by anchoring to the surrounding concrete to which they transfer, by bond, the force originating at their intersection with the CDC, O_i^l, as a result of the imposed end slip $\delta_{Li}[\gamma(t_n)]$, Fig. 1d. The capacity of each strip is provided by its available bond length L_{fi} that is the shorter between the two parts into which the crack divides its actual length L_f (Fig. 1a). Bond is the mechanism through which stresses are transferred to the surrounding concrete (Yuan *et al.* 2004, Mohammed Ali *et al.* 2006 and 2007, Bianco *et al.* 2009b). The local bond stress-slip relationship $\tau(\delta)$, comprehensively simulating the mechanical phenomena occurring at 1) the strip-adhesive interface, 2) within the adhesive layer and at 3) the adhesive-concrete interface, can be represented, in a simplified way, by a bi-linear curve (Fig. 1b). The subsequent phases undergone by bond during the loading process, representing the physical phenomena occurring in sequence within the adhesive layer by increasing the imposed end slip, are: “rigid”, “softening friction” and “free slipping” (Fig. 1b) (Bianco 2008). The first *rigid* branch (0-τ_0) represents the overall initial shear strength of the joint, independent

of the deformability of the adhesive layer and attributable to the micro-mechanical and mainly chemical properties of the involved materials and relative interfaces. In fact, the parameter τ_0 is the average of the following physical entities encountered in sequence by stresses flowing from the strip to the surrounding concrete, *i.e.*: adhesion at the strip-adhesive interface, cohesion within the adhesive itself, and adhesion at the adhesive-concrete interface (*e.g.* Sekulic and Curnier 2006, Zhai *et al.* 2008).

The $\tau(\delta)$ curve adopted (Fig. 1b) envisages that, by imposing an increasing end slip to the FRP strip, cracks form instantaneously within the adhesive layer, both orthogonally to the (inclined) tension isostatics and along the strip-adhesive and adhesive-concrete interfaces (*e.g.* Sena-Cruz and Barros 2004). Stresses are transferred by friction and micro-mechanical interlock along those micro-cracks. Nonetheless, by imposing an increasing end slip, those cracks progressively become smoother (*softening friction* phase) up to the point ($\delta_{Li} = \delta_1$) in which friction can no longer be mobilized and the strip is pulled out without having to overcome any restraint left (*free slipping* phase).

The constitutive law $V_{fi}\left(L_{Rfi};\delta_{Li}\right)$ of an NSM FRP strip, *i.e.* the force transmissible by a strip with resisting bond length L_{Rfi} as function of the imposed end slip δ_{Li}, can be determined by analyzing the behavior of the simple structural element composed of the NSM FRP strip within a concrete prism (Fig. 1a,c-d) whose transversal dimensions are limited by the spacing s_f between adjacent strips and half of the web cross section width $b_w/2$. In this way, the problem of interaction between adjacent strips (Dias and Barros 2008, Rizzo and De Lorenzis 2009) is taken into account in a simplified way, *i.e.*, by limiting the concrete volume into which subsequent fractures can form, to the amount of surrounding concrete pertaining to the single strip in dependence of s_f and b_w. Moreover, even though the interaction with existing stirrups is herein neglected, it may be also accounted for by limiting the transversal dimension of the concrete prism to a certain ratio of $b_w/2$, since the larger the amount of stirrups, the shallower concrete fracture is expected to be, even if further research is necessary in this respect.

Attention can be focused on the system composed of the strip with the average value of available bond length glued on the pertaining prism of surrounding concrete (Fig. 1c-d). The failure modes of an NSM FRP strip subject to an imposed end slip comprise, depending on the relative mechanical and geometrical properties of the materials involved: debonding, tensile rupture of the strip, concrete semi-pyramidal tensile fracture, and a mixed shallow-semi-pyramid-plus-debonding failure mode (Fig. 1e). The term *debonding* is adopted to designate loss of bond due to damage initiation and propagation within the adhesive layer and at the FRP strip-adhesive and adhesive-concrete interfaces, so that the strip pulling out results (Fig. 1e). When principal tensile stresses transferred to the

surrounding concrete attain its tensile strength, concrete fractures along a surface, envelope of the compression isostatics, whose shape can be conveniently assumed as a semi-pyramid with principal generatrices inclined of an angle α with respect to the strip longitudinal axis (Fig. 1c-d). Increasing the imposed end slip can result in subsequent semi-pyramidal and coaxial fracture surfaces in the concrete surrounding the NSM strip. This concrete fracture process progressively reduces the resisting bond length L_{Rfi} that is the portion of the initial available bond length L_{fi} still bonded to concrete. Those subsequent fractures can either progress up to the free end, resulting in a *concrete semi-pyramidal failure*, or stop progressing midway between loaded and free end, resulting in a *mixed-shallow-semi-pyramid-plus-debonding* failure (Fig. 1e). Moreover, regardless of an initial concrete fracture, the strip can *rupture* (Fig. 1e).

This modeling strategy can be further simplified introducing the following assumptions: 1) concrete fracture can be accounted for determining the equivalent value of the average resisting bond length $\bar{L}_{Rfi}^{eq}$, which is the portion of the available average resisting bond length $\bar{L}_{Rfi}^{eq} = \eta \cdot \bar{L}_{Rfi}$ ($0 \le \eta \le 1$) that would still be adhered to surrounding concrete, as function of the concrete mechanical properties, after all the successive co-axial semi-pyramidal fracture surfaces have formed in the surrounding concrete, and 2) the post peak behavior of the bond-based constitutive law $V_{fi}^{bd}\left(\bar{L}_{Rfi}^{eq};\delta_{Li}\right)$ of the equivalent value of the average resisting bond length can be neglected. As to the first assumption, the value of concrete average tensile strength f_{ctm}^{*} for values larger than which concrete does not fracture at all ($\eta = 1$) can be determined by imposing the equality between the maximum value of force that $\bar{L}_{Rfi}$ can transfer through bond stresses, and the corresponding value of concrete semi-pyramidal fracture strength. In other words, instead of imposing an increasing value of imposed end slip δ_{Li} to $\bar{L}_{Rfi}$ and analyzing how it progressively reduces at the occurrence of successive co-axial concrete fractures (Bianco *et al.* 2011), one can assume that, if concrete does not fracture for the value of δ_{Li} in correspondence of which the force transferred through bond by $\bar{L}_{Rfi}$ has attained its maximum value, even more it will not fracture either for smaller values of δ_{Li}, or for larger values of δ_{Li}. This is due to the fact that the maximum value of force that $\bar{L}_{Rfi}$ can transfer through bond is attained for the value of δ_{Li} in correspondence of which the distribution of bond stresses has reached the strip free extremity, if $\bar{L}_{Rfi} \le L_{Rfe}$, and when the bond transfer length has matched the effective resisting bond length, if $\bar{L}_{Rfi} > L_{Rfe}$. For a null value of f_{ctm}, the assumption is made that concrete semi-pyramidal

successive co-axial fracture surfaces would reach the average available bond length free extremity resulting in $\bar{L}_{Rfi}^{eq} = 0$ ($\eta = 0$). It is also assumed that, for values of concrete tensile strength $0 < f_{ctm} < f_{ctm}^{*}$, the reduction factor η has a linear trend between zero and unit $0 \le \eta \le 1$ (Fig. 2).

The maximum value of the effective capacity $V_{fi,eff}^{\max}$, which is the maximum value of the average of the NSM FRP strip capacity along the CDC (Bianco *et al.* 2011), can be approximated, and lightly underestimated, neglecting the post peak behavior of the bond-based constitutive law of the equivalent resisting bond length.

In the following paragraphs the resulting analytical equations are firstly presented and then are applied to simulate some of the most recent experimental results. Moreover, Monte Carlo simulation are carried out in order to assess the sensitivity of the results provided by the proposed formulation to the value assumed by the input parameters.

Proposed design formula

The input parameters include (Fig. 1): beam cross-section web's depth h_w and width b_w; inclination angle of both CDC and strips with respect to the beam longitudinal axis, θ and β, respectively; strips spacing measured along the beam axis s_f; angle α between axis and principal generatrices of the semi-pyramidal fracture surface (Fig. 1c-d); concrete average compressive strength f_{cm}; FRP tensile strength f_{fu} and Young's modulus E_f; thickness a_f and width b_f of the strip cross-section, and values of bond stress τ_0 and slip δ_1 defining the adopted local bond stress-slip relationship (Fig. 1b).

The implementation of the proposed calculation procedure comprehends the following steps (Fig. 3): 1) evaluation of the average value of the available (resisting) bond length $\bar{L}_{Rfi}$ and of the minimum integer number $N_{f,\text{int}}^{l}$ of NSM strips that can effectively cross the CDC; 2) evaluation of various constants, both integration and geometric ones; 3) evaluation of the reduction factor η of the average value of the available (resisting) bond length and of the equivalent value of the average resisting bond length $\bar{L}_{Rfi}^{eq}$; 4) evaluation of the value of the imposed end slip δ_{Lu} in correspondence of which the peak value of the force transmissible through bond by the equivalent value of the resisting bond length $\bar{L}_{Rfi}^{eq}$ can be attained; 5) evaluation of the maximum effective capacity that a NSM of bond length $\bar{L}_{Rfi}^{eq}$ can attain during the beam loading process ($V_{fi,eff}^{\max}$), and 6) evaluation of the strips shear strength contribution V_f.

Average value of the available resisting bond length $\bar{L}_{Rfi}$ ***and minimum number of strips*** $N^{l}_{f,\mathrm{int}}$ ***effectively crossing the CDC***

The average value of the available bond length and the minimum integer number of strips effectively crossing the CDC can be evaluated as follows (Fig. 1):

$$\bar{L}_{Rfi} = \frac{h_w \cdot \sin\theta \cdot (\cot\theta + \cot\beta)}{4 \cdot \sin(\theta + \beta)} \tag{1}$$

$$N^{l}_{f,\mathrm{int}} = \text{round off}\left[h_w \cdot \frac{(\cot\theta + \cot\beta)}{s_f} \right] \tag{2}$$

Evaluation of Constants

It is necessary to calculate some constants, both geometrical and integration ones, characterizing the bond transfer mechanism of the adopted NSM system, composed of a certain type of FRP strips, adhesive and concrete (Bianco *et al.* 2011). The geometric constants encompass (Fig. 1):

$$L_p = 2 \cdot b_f + a_f \tag{3}$$

the effective perimeter of the strip cross section;

$$A_c = s_f \cdot \frac{b_w}{2} \tag{4}$$

the cross section area of the relevant prism of surrounding concrete; and

$$L_d = \frac{h_w}{\sin\theta} \tag{5}$$

the CDC length.

The mechanical constants encompass:

$$V_f^{tr} = a_f \cdot b_f \cdot f_{fu} \tag{6}$$

the strip tensile strength;

$$f_{ctm} = 1.4 \cdot ((f_{cm} - 8)/10)^{\frac{2}{3}} \tag{7}$$

concrete mean tensile strength; and

$$E_c = 2.15 \cdot 10000 \cdot (f_{cm}/10)^{\frac{1}{3}} \tag{8}$$

concrete's Young's modulus, where both E_c and f_{ctm} are herein evaluated by means of the formulae present in the CEB-FIP Model Code 1990, with f_{cm} in MPa.

The bond-modeling constants encompass (see the Appendix):

$$J_1 = \frac{L_p}{A_f} \cdot \left[\frac{1}{E_f} + \frac{A_f}{A_c \cdot E_c} \right];\ \frac{1}{\lambda^2} = \frac{\delta_1}{\tau_0 \cdot J_1};\ C_3 = \frac{V_f^{tr} \cdot J_1}{L_p \cdot \lambda} \tag{9}$$

that are integration constants regarding the bond transfer mechanism;

$$L_{Rfe} = \frac{\pi}{2 \cdot \lambda};\ V_{f1}^{bd} = \frac{L_p \cdot \lambda \cdot \delta_1}{J_1} \tag{10}$$

the effective resisting bond length L_{Rfe}, and the corresponding maximum bond force V_{f1}^{bd}.

Reduction factor η and equivalent value of the average resisting bond length $\bar{L}_{Rfi}^{eq}$

The reduction factor can be evaluated as follows:

$$\eta\left(s_f; b_w; f_{cm}; \bar{L}_{Rfi}\right) = \begin{cases} f_{ctm} / f_{ctm}^* & se \quad f_{ctm} < f_{ctm}^* \\ 1 & se \quad f_{ctm} \geq f_{ctm}^* \end{cases} \tag{11}$$

where:

$$f_{ctm}^* = \frac{L_p \cdot \lambda \cdot \delta_1 \cdot \sin\left(\lambda \cdot L_{Rfi}\right)}{J_1 \cdot \min\left(L_{Rfi} \cdot \tan\alpha; \frac{b_w}{2} \right) \cdot \min\left(s_f \cdot \sin\beta; 2 \cdot L_{Rfi} \cdot \tan\alpha \right)} \tag{12}$$

in which L_{Rfi} has to be set equal to:

$$L_{Rfi} = \begin{cases} \bar{L}_{Rfi} & if \quad \bar{L}_{Rfi} \leq L_{Rfe} \\ L_{Rfe} & if \quad \bar{L}_{Rfi} > L_{Rfe} \end{cases} \tag{13}$$

The value of f_{ctm}^* is the one corresponding, under the above simplifying assumptions, for a given average NSM system, to the limit condition of occurrence of concrete fracture.

The equivalent value of the average resisting bond length is given by:

$$\bar{L}_{Rfi}^{eq} = \bar{L}_{Rfi} \cdot \eta\left(s_f; b_w; f_{cm}; \bar{L}_{Rfi}\right) \tag{14}$$

Value of the imposed end slip δ_{Lu} in correspondence of which the peak value of the comprehensive constitutive law $V_{fi}\left(\bar{L}_{Rfi}^{eq}; \delta_{Li}\right)$ of the equivalent average resisting bond length $\bar{L}_{Rfi}^{eq}$ is attained

In case the maximum invariant value of force that a given NSM system, characterized by a given FRP strip, a given adhesive layer and concrete, can transfer through bond stresses V_{f1}^{db} is larger or equal to the strip tensile strength V_f^{tr}, the value of imposed end slip in correspondence of which the peak value of the constitutive law $V_{fi}\left(\bar{L}_{Rfi}^{eq}; \delta_{Li}\right)$ is assumed as the minimum between $\delta_{L1}\left(\bar{L}_{Rfi}^{eq}\right)$ and $\delta_{L1}\left(V_f^{tr}\right)$ (Fig. 2d), where $\delta_{L1}\left(\bar{L}_{Rfi}^{eq}\right)$ is the value of imposed

end slip in correspondence of which the bond-based constitutive law $V_{fi}^{bd}\left(\bar{L}_{Rfi}^{eq};\delta_{Li}\right)$ attains the peak value, and $\delta_{L1}\left(V_f^{tr}\right)$ is the value of the imposed end slip in which the bond transferred force equals the strip tensile strength ($V_f^{tr}=a_f\cdot b_f\cdot f_{fu}$).

The value of the imposed end slip δ_{Lu} in correspondence of which the peak force transmissible by the equivalent average resisting bond length $\bar{L}_{Rfi}^{eq}$ is attained, is given by:

$$\delta_{Lu}=\begin{cases}\delta_{L1}\left(\bar{L}_{Rfi}^{eq}\right) & se\quad V_{f1}^{bd}<V_f^{tr}\\ \min\left[\delta_{L1}\left(\bar{L}_{Rfi}^{eq}\right);\delta_{Li}\left(V_f^{tr}\right)\right] & se\quad V_{f1}^{bd}\geq V_f^{tr}\end{cases} \tag{15}$$

where:

$$\delta_{L1}\left(\bar{L}_{Rfi}^{eq}\right)=\begin{cases}\delta_1\cdot\left[1-\cos\left(\lambda\cdot\bar{L}_{Rfi}^{eq}\right)\right] & \text{for}\quad \bar{L}_{Rfi}^{eq}\leq L_{Rfe}\\ \delta_1 & \text{for}\quad \bar{L}_{Rfi}^{eq}>L_{Rfe}\end{cases} \tag{16}$$

and:

$$\delta_{Li}\left(V_f^{tr}\right)=\delta_1\cdot\left\{1-\cos\left[-\arcsin\frac{C_3}{\delta_1}\right]\right\} \tag{17}$$

Maximum effective capacity $V_{fi,eff}^{\max}$ of the NSM strip with equivalent average resisting bond length $\bar{L}_{Rfi}^{eq}$

The maximum effective capacity can be evaluated, neglecting the post peak behavior of the constitutive law, as follows (Bianco *et al.* 2011):

$$V_{fi,eff}^{\max}=V_{fi,eff}\left(\gamma_{\max}\right)=\frac{\delta_1\cdot A_2}{2\cdot L_d\cdot A_3\cdot\gamma_{\max}}\cdot\left[\frac{\pi}{2}-\arcsin\psi-\psi\cdot\sqrt{1-\psi^2}\right] \tag{18}$$

where:

$$A_2=\frac{L_p\cdot\lambda}{J_1};\ A_3=\frac{\sin(\theta+\beta)}{2\cdot\delta_1};\ \gamma_{\max}=\frac{2\cdot\delta_{Lu}}{L_d\cdot\sin(\theta+\beta)};\ \psi=1-A_3\cdot\gamma_{\max}\cdot L_d \tag{19}$$

Shear strength contribution provided by a system of NSM FRP strips

The actual V_f and design value V_{fd} of the NSM shear strength contribution, can be obtained as follows:

$$V_{fd}=\frac{1}{\gamma_{Rd}}\cdot V_f=\frac{1}{\gamma_{Rd}}\cdot\left(2\cdot N_{f,\text{int}}^{l}\cdot V_{fi,eff}^{\max}\cdot\sin\beta\right) \tag{20}$$

where γ_{Rd} is the partial safety factor, divisor of a capacity, that can be assumed as 1.1-1.2 according to the level of uncertainty affecting the input parameters but, in this respect, a reliability-based calibration is needed.

Formulation Appraisal

The proposed formulation was applied to the RC beams tested by Dias and Barros (2008), Dias *et al.* (2007), Dias (2008), Rizzo and De Lorenzis (2009), A.K.M. Anwarul Islam (2009), Rahal, K.N. (2010), Rahal and Rumaih (2011), Jalali *et al.* (2012) and Cisneros *et al.* (2012).

The beams tested in the first two experimental programs (series I and II) were T cross-section RC beams characterized by the same test set-up with the same ratio between the shear span and the beam effective depth ($a/d = 2.5$), the same amount of longitudinal reinforcement, the same kind of CFRP strips and epoxy adhesive and they differed for the concrete mechanical properties. In fact, the first experimental program (series I) was characterized by a concrete average compressive strength f_{cm} of 31.1 *MPa*, while the second (series II) f_{cm} =18.6 *MPa*. Both series presented different configurations of NSM strips, in terms of both inclination β and spacing s_f . The second program also included beams characterized by a different amount of existing steel stirrups (see Table 1). The beams tested in the third experimental program (series III) were characterized by the same test set up, but with a different shear aspect ratio ($a/d = 3.3$) and a higher concrete average compressive strength ($f_{cm} = 59.4\ MPa$). Some of them were also subjected to pre-cracking (their label includes a letter F).

Those beams are characterized by the following common geometrical and mechanical parameters: $b_w = 180\ mm$; $h_w = 300\ mm$; $f_{fu} = 2952\ MPa$ (for the series I and II) and $f_{fu} = 2848\ MPa$ (for the series III); $E_f = 166.6\ GPa$ (for the series I and II) and $E_f = 174.3\ GPa$ (for the series III); $a_f = 1.4\ mm$; $b_f = 10.0\ mm$. The CDC inclination angle θ adopted in the simulations by the proposed formulation, listed in Table 1, is the one experimentally observed by inspecting the crack patterns (Dias 2008). Note that the experimental observations confirm the expected trend according to which θ diminishes for increasing values of the ratio a/d (*e.g.* Bousselham and Chaalal 2004, Chao *et. al.* 2005). In fact, for some beams of the III series ($a/d = 3.3$), $\theta^{\exp}$ assumes values smaller than 45º and up to 20º (Table 1). In this respect, it has to be stressed that assuming $\theta = 45^{\circ}$ could result excessively conservative since, with respect to smaller values (*e.g.* $\theta = 20^{\circ}$), and other parameters being the same, the predicted NSM shear strength contribution decreases due to the fact that the number of strips effectively crossing the CDC diminishes (Bianco 2008). It would be necessary to develop rigorous equations to

evaluate the CDC inclination angle θ as function of 1) shear aspect ratio a/d and amount of both 2) NSM strips and 3) existing steel stirrups but, in this respect, further research is necessary.

The beams tested by Rizzo and De Lorenzis (2009) (series IV) were rectangular cross-section RC beams strengthened in shear by either bars (their label starts by NB) or strips (their label starts by NS) and tested under four point bending (Table 2). These beams were characterized by cross-section dimensions of $b_w = 200\ mm$ and $h_w = 210\ mm$, and the ratio between the shear span and the beam effective depth was $a/d = 3.0$. Concrete had average compressive strength of 29.3 MPa. The round CFRP bars have a 8 mm diameter cross-section and for improvement of the bond properties, the surface of this type of bar is spirally wound with a carbon fiber tow and sand coated. The tensile strength and modulus of elasticity of the bars were $f_{fu} = 2.21\,GPa$ and $E_f = 145.7\ GPa$, respectively. The strips, have a cross-section of dimensions $a_f = 2.0\ mm$ and $b_f = 16.0\ mm$, and mechanical properties of $f_{fu} = 2.07\ GPa$ and $E_f = 121.5\,GPa$. Two kinds of epoxy were employed to glue the NSM reinforcement, both two-component 100% solid non-sag tixotropic epoxy adhesive pastes obtained by mixing resin and hardener in a 3:1 weight ratio, differ by the values of tensile strength and modulus of elasticity and are indicated, in the beam codes, by a letter a or b. The tensile strength and the secant tensile elastic modulus presented values of $18.6\ MPa$ and $4.15\ GPa$, respectively, for the type-a adhesive, and values of $22.8\ MPa$ and $12.87\ GPa$ for the type-b. Since the experimentally observed value of the CDC inclination angle is not reported, in the simulation a value of 45° was assumed.

The beams tested by A.K.M. Anwarul Islam (2009) (series V) were rectangular cross-section RC beams strengthened in shear by CFRP round bars and tested under four point bending (Table 3). These beams were characterized by cross-section dimensions of $b_w = 254\ mm$ and $h_w = 305\ mm$, and the ratio between the shear span and the beam effective depth was $a/d = 2.34$. Concrete had average compressive strength of 49.75 MPa. The round CFRP bars have a 9 mm diameter cross-section and tensile strength and modulus of elasticity of the bars were $f_{fu} = 2.07\ GPa$ and $E_f = 124.0\ GPa$, respectively. CFRP bars are inclined of 90° with respect to the beam longitudinal axis and since the experimentally observed value of the CDC inclination angle is not reported, in the simulation a value of 45° was assumed.

The beams tested by Rahal (2010) and by Rahal and Rumaih (2011) (series VI) were T cross-section RC beams strengthened in shear by NSM bars either of steel (their label includes a letter R) or CFRP (their label includes a letter F) and tested under four point bending (Table 4). All the five tested beams contained two test regions each, one strengthened with CFRP bars and the other with conventional steel bars. Hence, a total of ten results are

reported. These beams were characterized by T cross-section dimensions of $b_w = 150\ mm$ and $h_w = 400\ mm$, while the flange was $380\ mm$ in width and $100\ mm$ in depth, and the ratio between the shear span and the beam effective depth was $a/d = 3.0$. Concrete average compressive strength ranged from $36.2\ MPa$ to $38.6\ MPa$. The epoxy resin used to grout the bars in the groves was "non-sag" resin. The NSM steel bars were characterized by yield tensile strength of $0.51\,GPa$, while the NSM FRP bars were 8 *mm* deformed TYFO® carbon FRP bars characterized by $f_{fu} = 1.90\,GPa$ and $E_f = 124.0\,GPa$. Since the experimentally observed value of the CDC inclination angle is not reported, in the simulation a value of 45° was assumed.

The beams tested by Jalali *et al.* (2012) (series VII) were rectangular cross-section RC beams strengthened in shear by Manually Made NSM FRP rods (MMFRPs) with (their label includes a letter A) and without an extremity anchorage (Table 5) and tested under three point bending. These particular kind of FRP rods were obtained by wrapping a dry carbon fiber sheet, which was pre impregnated with resin, around a 6 *mm* diameter wooden rod. These rods were characterized by $f_{fu} = 3.55\,GPa$ and $E_f = 235.0\,GPa$. The beams were rectangular cross-section with dimensions $b_w = 200\ mm$ and $h_w = 250\ mm$, and the ratio between the shear span and the beam effective depth was $a/d = 2.73$. Concrete average compressive strength was equal to $f_{cm} = 36.4\,MPa$. Since the experimentally observed value of the CDC inclination angle is not reported, in the simulation a value of 45° was assumed.

The beams tested by Cisneros *et al.* (2012) (series VII) were rectangular cross-section RC beams strengthened in shear by either bars (their label starts by B) or strips (their label starts by S) and tested under three point bending (Table 6). Beams cross-section dimensions were $b_w = 200\ mm$ and $h_w = 350\ mm$. Each beam was tested twice, once at each end, and the ratio between the shear span and the beam effective depth equal to $a/d = 2.9$. Concrete average compressive strength ranged from $f_{cm} = 22.84\,MPa$ to $f_{cm} = 29.11\,MPa$. The NSM FRP bars were characterized by 8 *mm* diameter, while the strips had cross section dimensions of $a_f = 2.5\ mm$ and $b_f = 15.0\ mm$. FRP mechanical properties were $f_{fu} = 2.5\,GPa$ and $E_f = 165.0\,GPa$. The resin used was MBrace Adhesive 220 for the bars and Masterflow 920 SF for the strips. Since the experimentally observed value of the CDC inclination angle is not reported, in the simulation a value of 45° was assumed.

The angle α was assumed equal to 28.5° for all the experimental programs, being the average of values obtained in a previous investigation (Bianco 2008) by back-analysis of experimental data. As to the value of α, due to its importance to the prediction accuracy of NSM shear strength contributions, further research is desirable. Concrete

average tensile strength f_{ctm} was calculated from the average compressive strength by means of the formulae of the CEB Fib Model Code 1990. The parameters characterizing the adopted local bond stress-slip relationship (Fig. 1b) are for all the experimental programs: $\tau_0 = 20.1\,MPa$ and $\delta_1 = 7.12\,mm$. Those values were obtained by the values characterizing the more sophisticated local bond stress-slip relationship adopted in previous works (Bianco *et al.* 2009a, 2010), by fixing the value of $\tau_0 = 20.1\,MPa$ and determining $\delta_1 = 7.12\,mm$ by equating the fracture energy. In this respect, it has to be underlined that the necessity is felt to develop rigorous equations that would allow the values (τ_0, δ_1) characterizing the local bond stress slip relationship to be determined on the basis of: a) superficial chemical and micro-mechanical properties of FRP, adhesive and concrete, and b) the adhesive layer thickness. Nonetheless, further research is, in this respect, required. However, as highlighted by means of parametric studies (Bianco 2008), for the values of concrete mechanical properties that can be met in practice, debonding rarely occurs due the high capacity of currently available structural adhesives. Thus, slight variations of the values of the parameters τ_0 and δ_1 cannot be felt, in terms of NSM shear strength contribution, due to the premature occurrence of other failure modes such as either concrete fracture or strip rupture. For this reason, adopting values of $\tau_0 = 20.1\,MPa$ and $\delta_1 = 7.12\,mm$ for cases characterized by different values of both 1) superficial chemical-mechanical properties of FRP, adhesive and concrete, and 2) adhesive thickness, is not expected to significantly affect the predictive performance of the proposed formulation.

When NSM round bars are employed instead of strips, the equivalent square cross-section is employed in the calculations. In the case of the MMFRPs adopted by Jalali *et al.* (2012), since the FRP cross-section is an annulus, the corresponding area is adopted to evaluate A_f (with $A_f = 50.27\,mm^2$ obtaining $a_f = b_f = 7.10\,mm$). The same values of the equivalent square cross section dimensions are adopted to evaluate the effective perimeter $L_p = 2 \cdot b_f + a_f$, even though slightly underestimating this latter.

Note also that, for the works among those adopted as basis of the model appraisal, not reporting directly the NSM shear strength contribution $V_f^{\exp}$, this latter has been herein obtained as the difference between the shear strength of the strengthened beam and that of the control beam. Note also that in Tables 1-6, the symbol h_w has been adopted to indicate also the vertical height of the NSM bars, when they are coincident while, when the NSM bar is inserted through the flange thickness, the symbol h_f has been adopted instead.

The predictions obtained by the formulation proposed in the present work have also been compared with those obtained by the previous two more sophisticated versions of the same modeling strategy. The predictions obtained

by the first model (Bianco *et al.* 2009a), which contemplates three geometrical configurations that the occurred CDC can assume with respect to the system of NSM FRPs, are labeled by $V_{f,1}^{I}$, $V_{f,2}^{I}$ and $V_{f,3}^{I}$. The predictions obtained by the second and simplified model (Bianco *et al.* 2011) are labeled by V_f^{II} while those obtained by the third, further simplified model herein presented are labeled by V_f^{III}. The experimental results concerning beams 2S-8LI45-I and 4S-7LV-II have been neglected in the considerations below since they are deemed affected by some disturbance.

The formulation herein proposed provides, in general, satisfactory estimates of the experimental recordings $V_f^{\exp}$ since the ratio $V_f^{III}/V_f^{\exp}$ presents altogether mean value and standard deviation equal to 0.69 and 0.29, respectively. The second version of the adopted modeling strategy also provides satisfactory estimates of the experimental recordings $V_f^{\exp}$ since the ratio $V_f^{II}/V_f^{\exp}$ presents altogether mean value and standard deviation equal to 0.67 and 0.29, respectively, even it is not closed form and requires the implementation of an iterative procedure to determine the average resisting bond length strip's constitutive law. The first version of the adopted modeling strategy, much more sophisticated than the two more recent versions, provides much more satisfactory estimates. In fact, considering, for each analyzed beam, the closest prediction out of the three obtained, the ratio $V_f/V_f^{\exp}$ presents altogether mean value and standard deviation equal to 0.98 and 0.26, respectively, even if it is very cumbersome to be implemented and needs a stand-alone software to be developed.

Sensitivity analysis

A sensitivity analysis was carried out to assess the relative importance of each input parameter on the calculated value of the NSM shear strength contribution in order to figure out what are the input parameters that mostly affect the result. For this purpose, the proposed formulation, presented in the previous sections, was implemented in a spreadsheet that was re-calculated iteratively one hundred thousand times, each time with a set of new possible values of the input parameters. At each iteration, the new value of each parameter was sampled, independently from each other, from the relevant probability distribution assigned to it, and a new value of the output was generated in the corresponding cell. As simulation progressed, new possible outcomes were generated from each iteration and a numerical solver kept track of these output values. All of the input parameters (a_f, b_f, s_f, b_w, h_w, f_{cm}, α, f_{fu}, E_f, θ, τ_0, δ_1) were characterized by a uniform probability distribution, which means a range

of possible values with the same likelihood of occurrence (Table 7). These intervals cover the possible situations occurring in NSM shear strengthening interventions for RC beams.

In particular: the strip thickness a_f was characterized by a range of variation between 1.0 and $5.0\,mm$; the strip width b_f, the strips' spacing s_f, and the concrete average compressive strength f_{cm} were characterized by ranges of variation $5-35\,mm$, $50-250\,mm$ and $10-90\,MPa$, respectively; beam cross-section web's depth h_w and width b_w were characterized by ranges of variation $300-700\,mm$ and $150-400\,mm$. The input parameters τ_0 and δ_1 were characterized by ranges of variation $10-30\,MPa$ and $2.0-15.0\,mm$, respectively.

At each iteration, the value of each input parameter was sampled from the relevant probability distribution by the Monte Carlo Sampling Technique (Law and Kelton 2000, Ang and Tang 1975). Monte Carlo simulations is simply a repeated process of generating deterministic solutions to a given problem; each solution corresponds to a set of deterministic values of the underlying random input parameters. In other words, a Monte Carlo simulation recalculates the worksheet in which the deterministic formulation was implemented, over and over, each time assuming a set of input parameters whose values are selected randomly from the probability distribution assigned to each of them.

The outcome of the above simulations, being the result of calculations in which all input parameters are characterized by a uniform probability distribution, is itself characterized by a probability distribution and can be represented both in terms of probability density and cumulated ascending probability (Fig. 4). From those results it arises that, for the range of variations herein assigned to the input parameters (Table 7): 1) the equivalent average resisting bond length strip's maximum effective capacity $V_{fi,eff}^{\max}\left(\bar{L}_{Rfi}^{eq}\right)$ varies between 0.0 and $40.8\,kN$ in $95\,\%$ of cases, and 2) the NSM FRP strips shear strength contribution varies between 0.0 and $514.0\,kN$ in $95\,\%$ of cases.

The sensitivity analysis between the output and the input variables was herein carried out evaluating, by the multivariate stepwise regression method (*e.g.* Draper and Smith 1966), the regression coefficients of the input variables (Fig. 4). The larger the coefficient, the larger the impact that particular input has on the calculated value. A positive coefficient, with bar extending to the right, indicates that this input has a positive impact, which means that increasing this input will increase the output, while the opposite happens if the coefficient is negative.

The values of the plotted regression coefficients (Fig. 4) indicate the increment of output for a standard deviation of the relevant input. For instance, h_w has a mapped coefficient of 86.50, meaning that an increase of μ fraction of a standard deviation of input parameter h_w yields an increase of $86.50\cdot\mu$ units (kN, not standard deviations)

of the output V_f . The standard deviation of sampled values of h_w is $115.35\,kN$ (Table 8) and, therefore, every unit increase of input h_w impacts the output positively by $86.50/115.35 = 0.75\,kN$.

From the sensitivity analysis it was found that the input parameters that mostly affect the value of $V_{fi,eff}^{\max}$ are, in decreasing order of impact, the angle α between axis and generatrices of the concrete fracture surface, the concrete average compressive strength f_{cm} , the beam cross section depth h_w , and the strips spacing s_f (Fig. 4). It was also observed that the value of V_f is mostly affected by the value of h_w , α , f_{cm} , and the CDC inclination angle θ (Fig. 4).

Conclusions

A design formulation to predict the NSM FRP strips shear strength contribution to a RC beam was derived from a previously developed numerical model, introducing some simplifications, such as: 1) assuming the phenomenon of concrete fracture just as a *reducer* of the average available resisting bond length, and evaluating a resulting equivalent average resisting bond length, and 2) neglecting the post peak behavior of the equivalent average resisting bond length's bond-based constitutive law in the evaluation of the strip's maximum effective capacity. The predictive performance of the formulation was appraised by considering some of the most recent experimental results available in literature. The formulation provided very satisfactory estimates of the experimental recordings, resulting the ratio of the prediction versus the experimental value characterized by a mean value and a standard deviation of 0.69 and 0.29, respectively.

The proposed formulation was subsequently employed to carry out Monte Carlo simulations sampling, at each iteration, the value of each input parameter from the relevant uniform probability distribution and independently from each other. The results of those simulations were adopted in order to figure out which input parameters mostly affect the prediction of the NSM FRP strips shear strength contribution to a RC beam. From this sensitivity it arises that the input parameters that mostly affect the NSM shear strength contribution prediction are, in decreasing order of importance: h_w , α , f_{cm} and the CDC inclination angle θ.

Acknowledgements

The authors of the present work wish to acknowledge the support provided by the "Empreiteiros Casais", S&P®, degussa® Portugal, and Secil (Unibetão, Braga). The study reported in this paper forms a part of the research program "PrePam", with reference number of PTDC/ECM/114511/2009, supported by FCT. Also, this work was

carried out under the auspices of the Italian DPC-ReLuis Project (repertory n. 540), Research Line 8, whose financial support is greatly appreciated.

Notation

A_c = area of the concrete prism cross section

A_f = area of the strip's cross section

A_2 = integration constant entering the expressions to evaluate the $V_{fi,eff}^{\max}$

A_3 = integration constant entering the expressions to evaluate the $V_{fi,eff}^{\max}$

C_3 = integration constant for the softening friction phase

E_c = concrete Young's modulus

E_f = strips' CFRP Young's modulus

J_1 = bond modeling constant

L_d = CDC length

$\bar{L}_{Rfi}$ = average available resisting bond length

L_p = effective perimeter of the strip cross section

L_{Rfi} = *i*-th strip resisting bond length

L_{Rfe} = Effective resisting bond length

$\bar{L}_{Rfi}^{eq}$ = Equivalent average resisting bond length

$N_{f,\text{int}}^{l}$ = minimum integer number of strips that can effectively cross the CDC

$OXYZ$ = crack plane reference system

$O_i^l X_i^l$ = reference axis along the *i*-th strip available bond length L_{fi}

V_{fi}^{cf} = progressive concrete tensile fracture capacity along the *i*-th strip

V_{f1}^{db} = Maximum value of force transferable through bond by the given FRP NSM system

$V_{fi,eff}^{\max}$ = maximum effective capacity

$V_f^{\exp}$ = experimental value of the NSM shear strengthening contribution

V_f^{tr} = Strip tensile rupture capacity

V_f = actual value of the NSM shear strengthening contribution

V_{fd}	=	design value of the NSM shear strengthening contribution
$V_{fi}\left(\bar{L}_{Rfi};\delta_{Li}\right)$	=	comprehensive constitutive law of the average available resisting bond length
$V_{fi}^{bd}\left(\bar{L}_{Rfi};\delta_{Li}\right)$	=	bond-based constitutive law of the average available resisting bond length
a_f	=	strip cross section's thickness
b_f	=	strip cross section's width
b_w	=	beam cross section's width
f_{cm}	=	concrete average cylindrical compressive strength
f_{ctm}	=	concrete average tensile strength
f_{ctm}^{*}	=	Value of concrete average tensile strength for values larger than which concrete fracture does not occur
f_{fu}	=	FRP tensile strength
h_w	=	beam web height
h_f	=	vertical height of the NSM bar
s_f	=	spacing between adjacent strips along the beam axis
α	=	angle defining the concrete fracture surface
β	=	FRP strips inclination angle with respect to the beam longitudinal axis
δ_1	=	slip corresponding to the end of softening friction
δ_{Li}	=	imposed slip at the loaded extremity of the *i*-th strip
δ_{Lu}	=	imposed slip in correspondence of which the comprehensive peak force transmissible by $\bar{L}_{Rfi}^{eq}$ is attained
$\delta_{L1}\left(V_f^{tr}\right)$	=	Value of imposed end slip in correspondence of which the strip tensile strength is attained
$\delta_{L1}\left(L_{Rfi}\right)$	=	value of δ_{Li} defining the end of the first phase of the bond-based constitutive law
$\gamma_{\max}$	=	CDC opening angle for which the maximum effective capacity is attained
η	=	reduction factor of the initial average available resisting bond length
γ_{Rd}	=	partial safety factor divisor of the capacity
λ	=	constant entering the governing differential equation for elastic phase

θ	=	critical Diagonal Crack (CDC) inclination angle
$\theta^{\exp}$	=	experimentally observed CDC inclination angle
$\tau(\delta)$	=	local bond stress-slip relationship
ψ	=	Constant necessary to evaluate the maximum effective capacity provided by the equivalent average resisting bond length
τ_0	=	adhesive-cohesive initial bond strength

References

Ang, A., H-S, Tang, (1975), "Probability Concepts in Engineering Planning and Design – Volume I – Basic Principles", John Wiley & Sons, New York.

Ang, A., H-S, Tang, (1975), "Probability Concepts in Engineering Planning and Design – Volume II – Decision, Risk and Reliability", John Wiley & Sons, New York.

Bianco, V., Barros, J.A.O., Monti, G., (2009a). "Three dimensional mechanical model for simulating the NSM FRP strips shear strength contribution to RC beams", Engineering Structures, 31(4), April 2009, 815-826.

Bianco, V., Barros, J.A.O., Monti, G., (2009b). "Bond Model of NSM FRP strips in the context of the Shear Strengthening of RC beams", ASCE Journal of Structural Engineering, 135(6), June 2009.

Bianco, V., Barros, J.A.O., Monti, G., (2010). "New approach for modeling the contribution of NSM FRP strips for shear strengthening of RC beams", ASCE Journal of Composites for Construction, 14(1), January/February 2010.

Bianco, V., (2008). "Shear Strengthening of RC beams by means of NSM FRP strips: experimental evidence and analytical modeling", PhD Thesis, Dept. of Structural Engrg. and Geotechnics, Sapienza University of Rome, Italy, submitted on December 2008.

Bianco, V., Monti, G., Barros, J.A.O., (2011). "Theoretical model and computational procedure to evaluate the NSM FRP strips shear strength contribution to a RC beam", ASCE Journal of Structural Engineering, 137(11), November 2011.

Bousselham A., Chaalal O., (2004) "Shear Strengthening Reinforced Concrete Beams with Fiber-Reinforced Polymer: Assessment of Influencing Parameters and Required Research", ACI Structural Journal, Vol.101, Nº2, March-April, pp. 219-227.

CEB-FIP Model Code 90, (1993) Bulletin d'Information N° 213/214, Final version printed by Th. Telford, London, (1993; ISBN 0-7277-1696-4; 460 pages).

Chao S.Y., Chen J.F., Teng J.G., Hao Z., Chen J., (2005) "Debonding in Reinforced Concrete Beams Shear Strengthened with Complete Fiber Reinforced Polymer Wraps", Journal of Composites for Construction, ASCE September/October 2005/1.

Cisneros, D., Arteaga, A., De Diego, A., Alzate, A., Perera, R., (2012), "Experimental study on NSM FRP shear retrofitting of RC beams", 6th international conference on Composites in Civil Engineering, CICE 2012, Rome, Italy, 13-15 June 2012.

Dias, S.J.E. (2008). “Experimental and anlytical research in the shear strengthening of reinforced concreet beams using the near surface mounted technique with CFRP strips”, PhD Thesis, Department of Civil Engineering, University of Minho, Guimarães-Portugal, in Portuguese.

Dias, S.J.E., Bianco, V., Barros, J.A.O., Monti, G., (2007). “Low strength concrete T cross section RC beams strengthened in shear by NSM technique”, Workshop-Materiali ed Approcci Innovativi per il Progetto in Zona Sismica e la Mitigazione della Vulnerabilità delle Strutture, University of Salerno, Italy, 12-13 February.

Dias, S.J.E. and Barros, J.A.O., (2008). “Shear Strengthening of T Cross Section Reinforced Concrete Beams by Near Surface Mounted Technique”, Journal of Composites for Construction, ASCE, Vol. 12, No. 3, pp. 300-311.

Draper, N.R., and Smith, H., (1966). “Applied Regression Analysis”, New York: John Wiley & Sons, Inc. Chapter 6.

Islam, Anwarul, A.K.M., (2009). “Effective methods of using CFRP bars in shear strengthening of concrete girders”, Engineering Structures, 31(2009), 709-714.

Jalali, M., Sharbatdar, M.K., Chen, Jian-Fei, Alaee, Farshid Jandaghi, (2012), “Shear strengthening of RC beams using innovative manually made NSM FRP bars”, Construction and Building Materials, 36, 990-1000.

Law, A.M. and Kelton, W.D. Simulation Modeling and Analysis: McGraw-Hill, New York, NY, 1991,1982, 2000.

Monti, G., Renzelli, M., Luciani, P., (2003) “FRP Adhesion to Uncracked and Cracked Concrete Zones”, Proceedings of the 6th International Symposium on Fibre-Reinforced Polymer (FRP) Reinforcement for Concrete Structures (FRPRCS-6), Singapore, July, 183-192.

Monti, G., Santinelli, F., Liotta, M.A., (2004) “Mechanics of FRP Shear Strengthening of RC beams”, Proc. ECCM 11, Rhodes, Greece.

Monti, G., Liotta, M.A., (2007) “Tests and design equations for FRP-strengthening in shear”, Construction and Building Materials (2006), 21(4), April 2007, 799-809.

Mohammed Ali, M.S., Oehlers, D.J., Seracino, R. (2006). “Vertical shear interaction model between external FRP transverse plates and internal stirrups”, Engineering Structures 28, 381-389.

Mohammed Ali, M.S., Oehlers, D.J., Griffith, M.C., Seracino, R. (2007). “Interfacial stress transfer of near surface-mounted FRP-to-concrete joints”, Engineering Structures 30, 1861-1868.

Rahal, K.N., (2010). "Near surface mounted shear strengthening of reinforced concrete beams," American Concrete Institute, Special Publication SP-272-13, Oct. 2010, pp. 251-268

Rahal, Khaldoun N., Rumaih, Hantem A., (2011), “Tests on reinforced concrete beams strengthened in shear using near surface mounted CFRP and steel bars”, Engineering Structures, 33, 53-62.

Rizzo, A. and De Lorenzis, L., (2009) “Behaviour and capacity of Rc beams strengthened in shear with NSM FRP reinforcement”, Construction and Building Materials, Vol. 3, n. 4, April 2009, 1555-1567.

Sekulic, A., Curnier, A., (2006). “An original epoxy-stamp on glass-disc specimen exhibiting stable debonding for identifying adhesive properties between glass and epoxy”, International Journal of Adhesion and Adhesives, Vol. 27, pp. 611-620.

Sena-Cruz, J.M., Barros, J.A.O., (2004). “Bond between near-surface mounted CFRP laminate strips and concrete in structural strengthening”, Journal of Composites for Construction, ASCE, Vol. 8, No. 6, pp. 519-527.

Yuan, H., Teng, J.G., Seracino, R., Wu, Z.S., Yao, J. (2004). “Full-range behavior of FRP-to-concrete bonded joints”, Engineering Structures, 26, 553-565.

Zhai, L.L., Ling, G.P., Wang, Y.W., (2008). “Effect of nano-Al_2O_3 on adhesion strength of epoxy adhesive and steel”, International Journal of Adhesion and Adhesives, Vol. 28, No. 1-2, pp. 23-28.

TABLE CAPTIONS

Table 1. Values of the parameters characterizing the beams tested by Dias and Barros (2008), Dias *et al.* (2007) and Dias (2008).

Table 2. Values of the parameters characterizing the beams tested by Rizzo and De Lorenzis (2009).

Table 3. Values of the parameters characterizing the beams tested by A.K.M. Anwarul Islam (2009).

Table 4. Values of the parameters characterizing the beams tested by Rahal and Rumaih (2011) and by Rahal (2010).

Table 5. Values of the parameters characterizing the beams tested by Jalali *et al.* (2012).

Table 6. Values of the parameters characterizing the beams tested by Cisneros *et al.* (2012).

Table 7. Values characterizing the uniform probability distribution of the input parameters.

Table 8. Detailed statistics of both the sampled values of input parameters and the calculated output.

Table 1. Values of the parameters characterizing the beams tested by Dias and Barros (2008), Dias *et al.* (2007) and Dias (2008).

Beam Label	θ^{exp} °	β °	s_f *mm*	Steel Stirrups	$V_{f,1}^{I}$ *kN*	$V_{f,2}^{I}$ *kN*	$V_{f,3}^{I}$ *kN*	V_f^{II} *kN*	V_f^{exp} *kN*	V_f^{III} *kN*	V_f^{III}/V_f^{exp}
2S-3LV-I	40	90	267	ϕ6/300	18.53	6.46	55.33	10.77	**22.20**	**11.07**	**0.50**
2S-5LV-I	40	90	160	"	52.33	26.42	55.34	30.97	**25.20**	**22.15**	**0.88**
2S-8LV-I	36	90	100	"	68.58	58.88	64.33	29.59	**48.60**	**44.30**	**0.91**
2S-3LI45-I	45	45	367	"	35.10	15.41	45.73	23.44	**29.40**	**16.00**	**0.54**
2S-5LI45-I	45	45	220	"	46.11	49.14	45.74	23.19	**41.40**	**32.00**	**0.77**
2S-8LI45-I	36	45	138	"	75.89	79.71	78.73	59.55	**40.20***	**67.87**	**1.69**
2S-3LI60-I	33	60	325	"	50.69	18.90	51.68	30.74	**35.40**	**12.88**	**0.36**
2S-5LI60-I	36	60	195	"	36.37	36.59	48.55	22.27	**46.20**	**38.65**	**0.84**
2S-7LI60-I	33	60	139	"	52.98	63.07	67.58	60.80	**54.60**	**51.53**	**0.94**
2S-7LV-II	46	90	114	ϕ6/300	26.72	31.84	35.59	15.04	**28.32**	**13.19**	**0.47**
2S-4LI45-II	40	45	275	"	25.06	21.89	37.30	19.24	**33.90**	**19.09**	**0.56**
2S-7LI45-II	30	45	157	"	49.36	47.13	45.95	37.92	**48.00**	**46.02**	**0.96**
2S-4LI60-II	40	60	243	"	21.31	15.04	29.38	13.23	**33.06**	**15.35**	**0.46**
2S-6LI60-II	27	60	162	"	42.79	37.54	39.45	34.68	**42.72**	**30.70**	**0.72**
4S-7LV-II	46	90	114	ϕ6/180	26.72	31.84	35.59	15.04	**6.90***	**13.19**	**1.91**
4S-4LI45-II	40	45	275	"	25.06	21.89	37.30	19.24	**26.04**	**19.09**	**0.73**
4S-7LI45-II	40	45	157	"	40.58	37.48	40.63	28.36	**31.56**	**36.82**	**1.17**
4S-4LI60-II	40	60	243	"	21.31	15.04	29.38	13.23	**25.08**	**15.35**	**0.61**
4S-6LI60-II	30	60	162	"	38.92	35.46	36.71	25.72	**35.10**	**30.70**	**0.87**
3S-5LI45-III	30	45	275	ϕ6/300	59.74	59.55	70.01	70.33	**66.10**	**54.03**	**0.82**
3S-5LI45F1-III**	23	45	275	"	83.05	86.96	81.15	77.93	**85.75**	**81.05**	**0.95**
3S-5LI45F2-III**	30	45	275	"	59.74	59.55	70.01	70.33	**65.35**	**54.03**	**0.83**
5S-5LI45-III	28	45	275	ϕ6/200	78.24	59.55	72.01	57.76	**74.90**	**81.05**	**1.08**
5S-5LI45F-III**	28	45	275	"	78.24	59.55	72.01	57.76	**74.90**	**81.05**	**1.08**
3S-9LI45-III	32	45	157	ϕ6/300	109.88	109.32	98.30	114.30	**101.85**	**104.27**	**1.02**
5S-9LI45-III	32	45	157	ϕ6/200	109.88	109.32	98.30	114.30	**108.90**	**104.27**	**0.96**
3S-5LI60-III	26	60	243	ϕ6/300	71.74	76.20	62.81	52.84	**69.00**	**65.61**	**0.95**
5S-5LI60-III	25	60	243	ϕ6/200	68.48	77.44	63.79	59.82	**73.35**	**65.61**	**0.89**
5S-5LI60F-III**	25	60	243	"	68.48	77.44	63.79	59.82	**72.55**	**65.61**	**0.90**
3S-8LI60-III	22	60	162	ϕ6/300	112.82	119.58	112.25	109.30	**112.30**	**109.35**	**0.97**
5S-8LI60-III	19	60	162	ϕ6/200	123.34	122.74	132.00	114.69	**122.45**	**131.22**	**1.07**
3S-6LV-III	45	90	180	ϕ6/300	58.24	26.62	66.53	35.04	**39.58**	**18.83**	**0.48**
3S-10LV-III	32	90	114	"	97.50	82.41	85.21	60.23	**83.25**	**75.34**	**0.90**

* beams whose experimental value of NSM shear strength contribution is affected by some disturbance;

** beams that were subjected to pre-cracking.

Table 2. Values of the parameters characterizing the beams tested by Rizzo and De Lorenzis (2009).

Beam Label	θ °	β °	s_f *mm*	f_{fu} *GPa*	E_f *GPa*	a_f *mm*	b_f *mm*	ϕ_f *mm*	$V_{f,1}^I$ *kN*	$V_{f,2}^I$ *kN*	$V_{f,3}^I$ *kN*	V_f^{II} *kN*	V_f^{exp} *kN*	V_f *kN*	V_f / V_f^{exp}
NB90-73-a-IV	45	90	73	2.21	145.7	-	-	8	24.84	27.01	33.73	11.59	**54.20**	**10.08**	**0.19**
NB90-73b-IV	45	90	73	"	"	-	-	"	24.84	27.01	33.73	11.59	**26.40**	**10.08**	**0.38**
NB90-45-b-IV	45	90	45	"	"	-	-	"	35.86	31.77	38.87	16.99	**28.60**	**15.92**	**0.56**
NB45-146-a-IV	45	45	146	"	"	-	-	"	25.50	24.69	24.69	17.68	**39.10**	**14.31**	**0.37**
NB45-73-a-IV	45	45	73	"	"	-	-	"	37.69	34.06	38.86	19.54	**28.00**	**22.91**	**0.82**
NS90-73-a-IV	45	90	73	2.07	121.5	2.0	16.0	-	21.39	23.98	34.24	12.93	**50.50**	**10.16**	**0.20**
NS45-146-a-IV	45	45	146	"	"	"	"	-	27.76	27.87	34.33	14.09	**32.70**	**14.53**	**0.44**

b_w 200 mm; h_w 210 mm; f_{cm} 29.3 MPa; steel stirrups ⌽6/160;

Table 3. Values of the parameters characterizing the beams tested by A.K.M. Anwarul Islam (2009).

Beam Label	θ °	β °	s_f *mm*	Steel Stirrups	f_{fu} *GPa*	E_f *GPa*	$V_{f,1}^{I}$ *kN*	$V_{f,2}^{I}$ *kN*	$V_{f,3}^{I}$ *kN*	V_f^{II} *kN*	$V_f^{\exp}$ *kN*	V_f *kN*	$V_f / V_f^{\exp}$
B2-FRP-V	45	90	152	-	2.07	124	77.16	43.65	77.57	28.98	**44.50**	**33.44**	**0.75**
B-3-FRP-V	45	90	305	ϕ9/305	2.07	124	0.00	0.00	77.11	1.16	**31.00**	**16.72**	**0.54**
B-4-FRP-V	45	90	191	ϕ9/610	2.07	124	49.76	28.79	77.53	37.26	**35.50**	**16.72**	**0.47**

b_w 254 *mm*; h_w 305 *mm*; ϕ_f 9.0 *mm*; f_{cm} 49.75 *MPa*;

Table 4. Values of the parameters characterizing the beams tested by Rahal and Rumaih (2011) and by Rahal (2010).

Beam Label	θ °	β °	s_f *mm*	f_{fu} *GPa*	f_{cm} *MPa*	E_f *GPa*	h_f *mm*	$V_{f,1}^{I}$ *kN*	$V_{f,2}^{I}$ *kN*	$V_{f,3}^{I}$ *kN*	V_f^{II} *kN*	$V_f^{\exp}$ *kN*	V_f^{III} *kN*	$V_f^{III}/V_f^{\exp}$
B2-B90-R200-VI	45	90	200	0.51	37.3	210	400	51.42	68.16	51.42	47.10	**55.0**	**45.47**	**0.83**
B2-B90-F200-VI	45	90	"	1.90	"	124	"	87.39	71.92	87.39	27.36	**70.0**	**45.73**	**0.65**
B3-B90-R200A-VI	45	90	"	0.51	37.8	210	500	71.51	85.06	57.82	64.41	**83.0**	**68.63**	**0.83**
B3-B90-F200A-VI	45	90	"	1.90	"	124	"	135.25	130.47	111.49	73.28	**103.0**	**72.74**	**0.71**
B4-B45-R200-VI	45	45	"	0.51	36.2	210	400	88.94	69.08	88.94	53.13	**113.0**	**97.06**	**0.86**
B4-B45-F200-VI	45	45	"	1.90	"	124	"	120.20	97.67	120.20	107.60	**138.0**	**114.85**	**0.83**
B5-B45-R200L-VI	45	45	"	0.51	38.6	210	"	90.51	69.37	90.51	97.10	**85.0**	**97.06**	**1.14**
B5-B45-F200L-VI	45	45	"	1.90	"	124	"	123.78	94.42	123.78	89.85	**115.0**	**121.2**	**1.05**
B6-B45-R300-VI	45	45	300	0.51	37.2	210	"	53.73	59.38	42.73	48.55	**40.0**	**48.53**	**1.21**
B6-B45-F300-VI	45	45	"	1.90	"	124	"	76.85	69.27	80.73	67.10	**55.0**	**63.73**	**1.16**

ϕ_f equal to 8 mm; b_w equal to 150 mm; steel stirrups equal to Φ6/200;

Table 5. Values of the parameters characterizing the beams tested by Jalali *et al.* (2012).

Beam Label	θ °	β °	s_f *mm*	Steel Stirrups	f_{fu} *GPa*	E_f *GPa*	$V_{f,1}^{I}$ *kN*	$V_{f,2}^{I}$ *kN*	$V_{f,3}^{I}$ *kN*	V_f^{II} *kN*	$V_f^{\exp}$ *kN*	V_f *kN*	$V_f / V_f^{\exp}$
VR-VII	45	90	160	⌽6/150	3.55	235	28.18	10.65	52.28	12.5	**33.41**	**8.65**	**0.26**
IR-VII	45	45	240	"	"	"	43.36	25.69	35.85	19.94	**53.94**	**24.54**	**0.45**
VRA-VII	45	90	160	"	"	"	28.18	10.65	52.28	12.5	**39.88**	**8.65**	**0.22**
IRA-VII	45	45	240	"	"	"	43.36	25.69	35.85	19.94	**63.82**	**24.54**	**0.38**
VRA-VII	45	90	160	"	"	"	28.18	10.65	52.28	12.5	**29.4**	**8.65**	**0.29**

b_w 200 *mm*; h_w 250 *mm*; f_{cm} 36.4 *MPa*; a_f b_f 3.46 *mm*

Table 6. Values of the parameters characterizing the beams tested by Cisneros *et al.* (2012).

Beam Label	θ °	β °	s_f *mm*	Steel Stirrups	f_{cm} *MPa*	a_f *mm*	b_f *mm*	ϕ_f *mm*	$V_{f,1}^{I}$ *kN*	$V_{f,2}^{I}$ *kN*	$V_{f,3}^{I}$ *kN*	V_f^{II} *kN*	$V_f^{\exp}$ *kN*	V_f *kN*	$V_f / V_f^{\exp}$
B90-6a-VIII	45	90	115	ϕ6/150	26.69	-	-	8	35.91	36.04	55.17	20.50	**58.30**	**18.91**	**0.32**
B90-6b-VIII	"	"	"	"	24.09	-	-	"	33.03	34.53	50.28	19.88	**55.00**	**17.12**	**0.31**
B90-3a-VIII	"	"	230	"	22.84	-	-	"	12.07	3.69	45.79	8.66	**11.00**	**8.11**	**0.74**
B90-3b-VIII	"	"	"	"	26.02	-	-	"	12.96	4.55	51.54	9.22	**6.30**	**9.23**	**1.47**
B45-6a-VIII	"	45	115	"	22.98	-	-	"	44.14	44.90	49.52	37.05	**74.20**	**41.02**	**0.55**
B45-6b-VIII	"	"	"	"	28.48	-	-	"	56.03	57.10	62.56	50.34	**98.20**	**50.52**	**0.51**
B45-3a-VIII	"	"	230	"	29.11	-	-	"	35.29	36.87	51.88	26.84	**40.20**	**29.19**	**0.73**
B45-3b-VIII	"	"	"	"	23.91	-	-	"	31.22	35.24	53.06	19.04	**81.00**	**24.18**	**0.30**
S90-6a-VIII	"	90	115	"	26.69	2.5	15.0	-	34.52	36.51	55.37	16.90	**75.80**	**19.05**	**0.25**
S90-6b-VIII	"	"	"	"	24.09	"	"	-	34.03	37.66	58.26	21.77	**38.90**	**17.24**	**0.44**
S90-3a-VIII	"	"	230	"	22.84	"	"	-	13.96	5.36	57.37	9.24	**10.50**	**8.17**	**0.78**
S90-3b-VIII	"	"	"	"	26.02	"	"	-	15.66	5.84	55.34	7.80	**20.40**	**9.3**	**0.46**
S45-6a-VIII	"	45	115	"	22.98	"	"	-	54.24	52.13	54.22	31.96	**77.10**	**41.63**	**0.54**
S45-6b-VIII	"	"	"	"	28.48	"	"	-	58.79	56.21	72.10	45.82	**106.40**	**51.27**	**0.48**
S45-3a-VIII	"	"	230	"	29.11	"	"	-	37.34	45.79	50.38	35.33	**58.10**	**29.62**	**0.51**
S45-3b-VIII	"	"	"	"	23.91	"	"	-	45.29	32.39	50.97	31.68	**98.00**	**24.54**	**0.25**

f_{fu} 2.5 *GPa*; E_f 165 *GPa*; b_w 200 mm; h_w 300 mm;

Table 7. Values characterizing the uniform probability distribution of the input parameters.

	θ °	h_w *mm*	b_w *mm*	a_f *mm*	b_f *mm*	s_f *mm*	β °	E_f *GPa*	f_{fu} *GPa*	f_{cm} *MPa*	α °	τ_0 *MPa*	δ_1 *mm*
Range of variation	20-60	300-700	150-400	1.0-5.5	5-35	50-250	45-90	100-200	1.0-6.0	10-90	10-35	10-30	2.0-15.0

Table 8. Detailed statistics of both the sampled values of input parameters and the calculated output.

	$V_{fi,eff}^{max}$ kN	V_f kN	θ °	h_w *mm*	b_w *mm*	a_f *mm*	b_f *mm*	s_f *mm*	β °	E_f *GPa*	f_{fu} *GPa*	f_{cm} *MPa*	α °	τ_0 *MPa*	δ_1 *mm*
Minimum	0.16	0	20.0	300.0	150.0	1.0	5.0	50.0	45.0	100.0	1.0	10.0	10.0	10.0	2.0
Maximum	123.42	1886.39	59.99	699.99	399.99	5.49	34.99	249.99	89.99	199.99	5.99	89.99	35.0	29.99	14.99
Mean	14.63	163.66	40.03	499.21	275.19	3.25	20.01	149.93	67.51	149.90	3.50	49.98	22.5	19.99	8.51
Standard Deviation	12.77	172.13	11.55	115.35	72.21	1.29	8.63	57.79	12.98	28.92	1.44	23.11	7.22	5.78	3.75

FIGURE CAPTIONS

Fig. 1. Main physical-mechanical features of the theoretical model and calculation procedure: a) average-available-bond-length NSM strip and concrete prism of influence, b) adopted local bond stress-slip relationship, c) NSM strip confined to the corresponding concrete prism of influence and semi-pyramidal fracture surface, d) sections of the concrete prism.

Fig. 2. Further simplifying assumptions introduced: a) reduction of the available average resisting bond length due to progressive concrete fracture, b) available length reduction factor as function of the concrete average tensile strength, c) bond-based constitutive law for NSM FRP strips with different values of resisting bond length, d) assumed comprehensive constitutive law of the equivalent average available resisting bond length strip.

Fig. 3. Calculation procedure: main algorithm.

Fig. 4. Results of the Monte Carlo simulations: probability density distribution, cumulated probability distribution and mapped regression coefficients for a) the NSM FRP strips shear strength contribution V_f , and b) the average strip maximum effective capacity $V_{fi,eff}^{\max}$.

Fig. A1. Evaluation of the average available resisting bond length $\overline{L}_{Rfi}$.

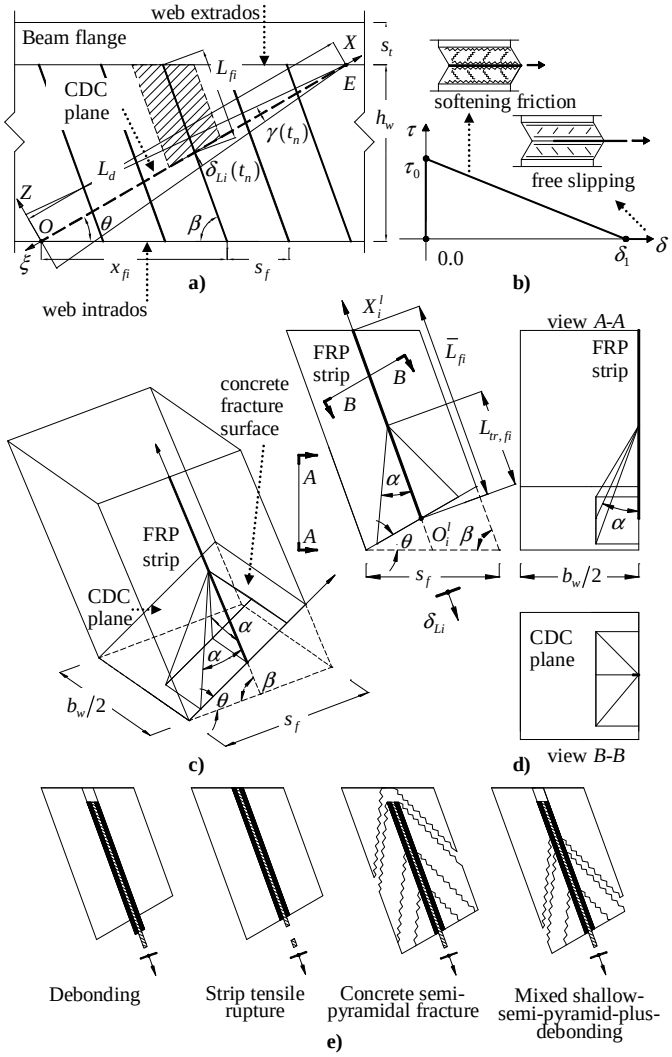

Fig. 1. Main physical-mechanical features of the theoretical model and calculation procedure: a) average-available-bond-length NSM strip and concrete prism of influence, b) adopted local bond stress-slip relationship, c) NSM strip confined to the corresponding concrete prism of influence and semi-pyramidal fracture surface, d) sections of the concrete prism.

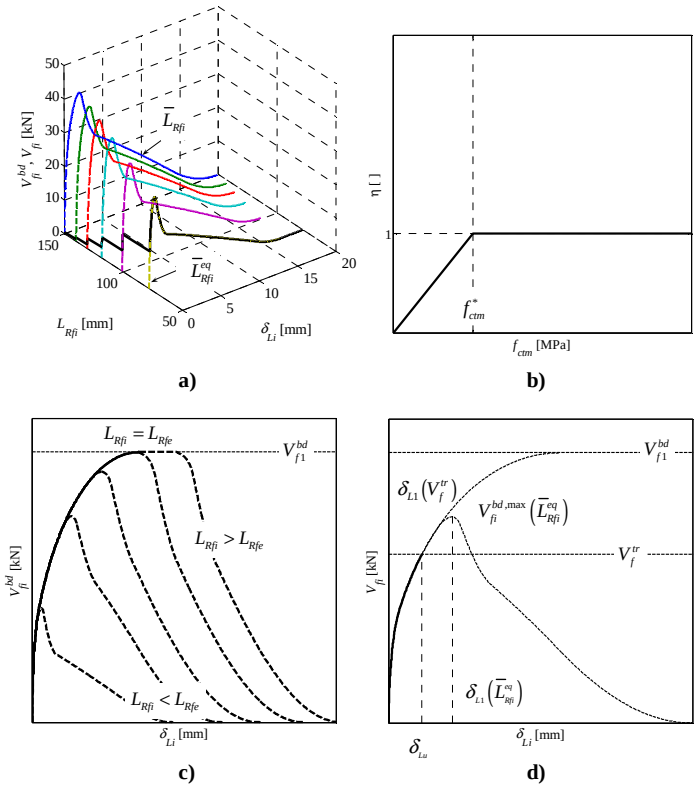

Fig. 2. Further simplifying assumptions introduced: a) reduction of the available average resisting bond length due to progressive concrete fracture, b) available length reduction factor as function of the concrete average tensile strength, c) bond-based constitutive law for NSM FRP strips with different values of resisting bond length, d) assumed comprehensive constitutive law of the equivalent average available resisting bond length strip.

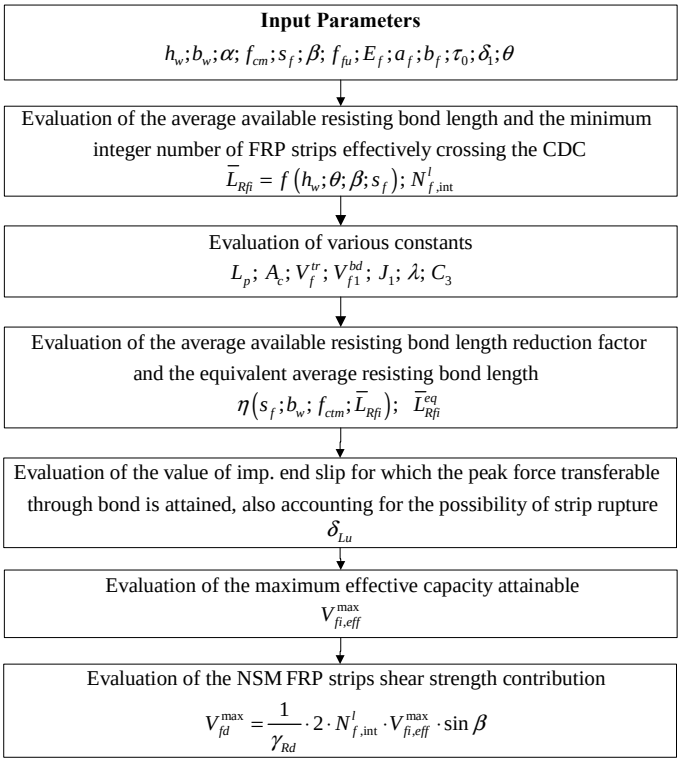

Fig. 3. Calculation procedure: main algorithm.

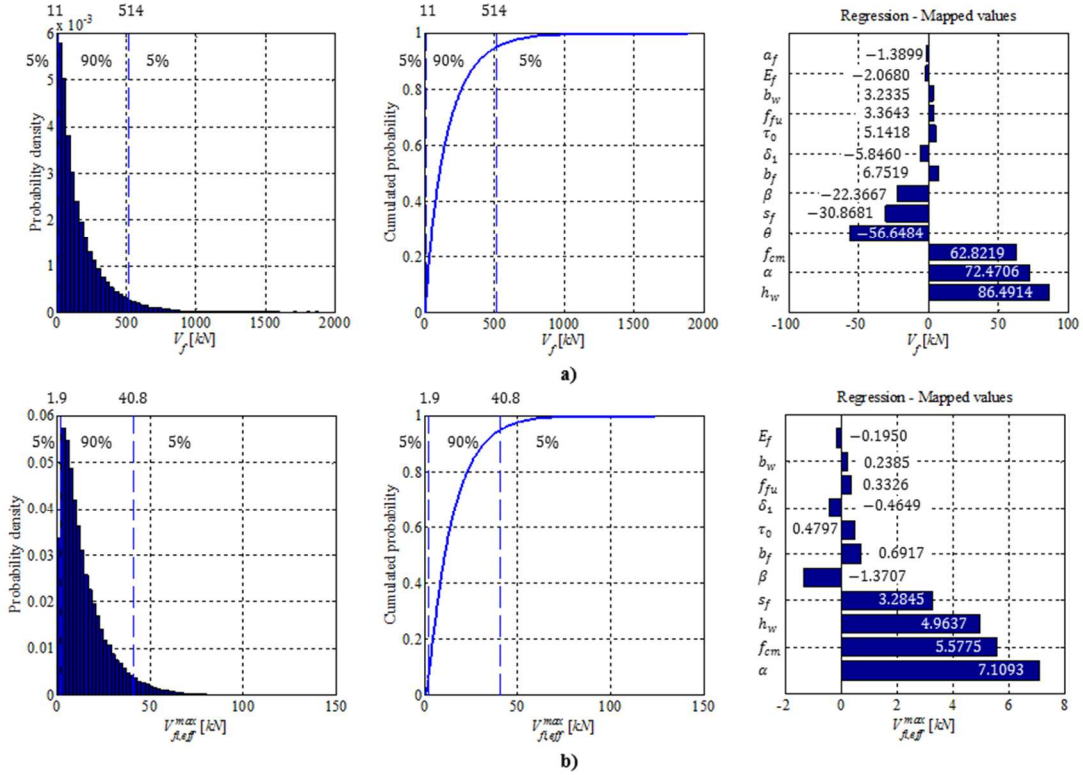

Fig. 4. Results of the Monte Carlo simulations: probability density distribution, cumulated probability distribution and mapped regression coefficients for a) the NSM FRP strips shear strength contribution V_f , and b) the average strip maximum effective capacity $V_{fi,eff}^{\max}$.

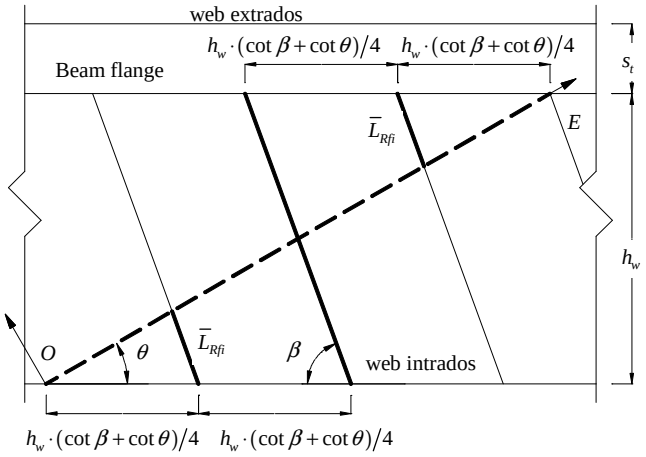

Fig. A1. Evaluation of the average available resisting bond length $\bar{L}_{Rfi}$.

APPENDIX

The average available resisting bond length herein is no longer evaluated as the average of the available resisting bond length $\bar{L}_{fi} = \sum_{i=1}^{N^l_{f,\text{int}}} L_{fi} \Big/ N^l_{f,\text{int}}$ of all the $N^l_{f,\text{int}}$ strips effectively bridging the CDC, as done in the previous work (Bianco *et al.* 2011). In an attempt to gain simplicity, without losing accuracy, $\bar{L}_{fi}$, herein designated as $\bar{L}_{Rfi}$, is evaluated as the actual average value that a strip effectively intersecting the CDC can attain, independently of either the actual number of strips and their location along the CDC. According to the approach schematically represented in Fig. A1, $\bar{L}_{Rfi}$ is evaluated by applying the sine theorem to the smallest triangle, *i.e.*: $\frac{\bar{L}_{Rfi}}{\sin\theta} = \frac{h_w \cdot (\cot\theta + \cot\beta)}{4 \cdot \sin[\pi - (\theta + \beta)]}$ from which Eq. (1) can be derived.

Once the value of the equivalent average resisting bond length $\bar{L}^{eq}_{Rfi}$ is evaluated, the relevant bond-based constitutive law $V^{bd}_{fi}\left(\bar{L}^{eq}_{Rfi}; \delta_{Li}\right)$ is considered neglecting the post-peak branch thus reducing, with respect to what was done in the previous work (Bianco *et al.* 2011), to:

$$V^{bd}_{fi}\left(\bar{L}^{eq}_{Rfi}; \delta_{Li}\right) = L_p \cdot J_3 \cdot \lambda \cdot \left\{C^{sf}_1 \cdot \left[\cos\left(\lambda \cdot L^{sf}_{tr}(\delta_{Li})\right) - 1\right] - C^{sf}_2 \cdot \sin\left(\lambda \cdot L^{sf}_{tr}(\delta_{Li})\right)\right\} \tag{A1}$$

To evaluate the value of imposed end slip in correspondence of which the force transferred through bond equals the strip rupture capacity V^{tr}_f, the $V^{bd}_{fi}\left(\bar{L}^{eq}_{Rfi}; \delta_{Li}\right)$ in the previous equations is replaced by V^{tr}_f:

$$\frac{V^{tr}_f}{L_p \cdot J_3 \cdot \lambda} = \cdot \left\{C^{sf}_1 \cdot \left[\cos\left(\lambda \cdot L^{sf}_{tr}(\delta_{Li})\right) - 1\right] - C^{sf}_2 \cdot \sin\left(\lambda \cdot L^{sf}_{tr}(\delta_{Li})\right)\right\} \tag{A2}$$

that can be rewritten as:

$$C^{sf}_1 \cdot \cos\left(\lambda \cdot L^{sf}_{tr}\right) - C^{sf}_2 \cdot \sin\left(\lambda \cdot L^{sf}_{tr}\right) = \frac{V^{tr}_f}{L_p \cdot J_3 \cdot \lambda} + C^{sf}_1 = C^{sf}_3 \tag{A3}$$

in which $L^{sf}_{tr}(\delta_{Li})$ was indicated, for the sake of brevity, as L^{sf}_{tr}. Moreover, since in the present work the superscript *sf* referring to the softening friction bond fase is neglected, the previous equation is reduced to:

$$C_1 \cdot \cos\left(\lambda \cdot L_{tr}\right) - C_2 \cdot \sin\left(\lambda \cdot L_{tr}\right) = \frac{V^{tr}_f}{L_p \cdot J_3 \cdot \lambda} + C_1 = C_3 \tag{A4}$$

This equation, in which the unknown is $\delta_{L1}\left(V_f^{tr}\right)$ that is the value of δ_{Li} such that $V_{fi}^{bd}\left(\overline{L}_{Rfi}^{eq};\delta_{Li}\right)=V_f^{tr}$, is solved as follows: each term is firstly divided by $\sqrt{C_1^2+C_2^2}$ and then the position in made in which $C_1\Big/\sqrt{C_1^2+C_2^2}=\sin\varphi$ and $C_2\Big/\sqrt{C_1^2+C_2^2}=\cos\varphi$, yielding:

$$\frac{C_3}{\sqrt{C_1^2+C_2^2}}=\sin\left(\varphi-\lambda\cdot L_{tr}\right) \tag{A5}$$

From this latter, one obtains:

$$L_{tr}=\frac{1}{\lambda}\cdot\left[\varphi-\arcsin\frac{C_3}{\sqrt{C_1^2+C_2^2}}\right] \tag{A6}$$

Introducing in this latter the expression the dependence of L_{tr} on δ_{Li}, given by Eq. (6.1) of the previous work (Bianco *et al.* 2011) the following equation is derived:

$$\frac{1}{\lambda}\cdot\arccos\left(1-\frac{\lambda^2}{\tau_0\cdot J_1}\cdot\delta_{Li}\right)=\frac{1}{\lambda}\cdot\left[\varphi-\arcsin\frac{C_3}{\sqrt{C_1^2+C_2^2}}\right] \tag{A7}$$

Making the cosine of both members, results:

$$\delta_{Li}\left(V_f^{tr}\right)=\frac{\tau_0\cdot J_1}{\lambda^2}\left\{1-\cos\cdot\left[\arcsin\frac{C_1}{\sqrt{C_1^2+C_2^2}}-\arcsin\frac{C_3}{\sqrt{C_1^2+C_2^2}}\right]\right\} \tag{A8}$$

where:

$$\begin{aligned}&\frac{1}{\lambda^2}=\frac{\delta_1}{\tau_0\cdot J_1};J_1=\frac{L_p}{A_f}\cdot\left[\frac{1}{E_f}+\frac{A_f}{A_c\cdot E_c}\right];J_2=\frac{E_f\cdot E_c\cdot A_c}{E_c\cdot A_c+E_f\cdot A_f}\\&J_3=\frac{E_f\cdot A_f\cdot E_c\cdot A_c}{L_p\cdot\left(A_c\cdot E_c+A_f\cdot E_f\right)};C_1=\delta_1-\frac{\tau_0\cdot J_1}{\lambda^2};C_2=-\frac{\tau_0\cdot J_1}{\lambda^2};C_3=\frac{V_f^{tr}}{L_p\cdot J_3\cdot\lambda}+C_1\end{aligned} \tag{A9}$$

Eq. (A8) gives a finite non null value only if $V_{f1}^{bd}\geq V_f^{tr}$ (compare Fig. 2). The above constants can be further simplified as follows:

since $J_3=\frac{1}{J_1}$, J_3 will be eliminated and substituted, whenever it appears, by $\frac{1}{J_1}$;

since $\frac{1}{\lambda^2}=\frac{\delta_1}{\tau_0\cdot J_1}$, C_1 vanishes and C_2 can be written as $C_2=-\delta_1$ so that, in the various expressions, only C_3 will be kept.

On the basis of the above simplifications, and since $\cos(angle)=\cos(-1\cdot angle)$, Eq. (A8) simplifies into:

$$\delta_{Li}\left(V_f^{tr}\right)=\delta_1\cdot\left\{1-\cos\cdot\left[\arcsin\frac{C_3}{\sqrt{C_1^2+C_2^2}}\right]\right\} \tag{A10}$$

As already stated in the paper, there must be a value f_{ctm}^{*} of concrete mean tensile strength beyond which concrete no longer fractures and the equivalent value of the average available resisting bond length is equal to the average available resisting bond length $\bar{L}_{Rfi}^{eq}=\bar{L}_{Rfi}\cdot 1.0$ .The value of f_{ctm}^{*} can be determined by imposing the equality $V_{fi,\max}^{cf}=V_{fi,\max}^{bd}$ between the concrete fracture capacity V_{fi}^{cf} and the corresponding maximum value of the bond transferred force V_{fi}^{bd} . This latter will be attained for a transfer length that is equal to $\bar{L}_{Rfi}$, if it is $\bar{L}_{Rfi}\le L_{Rfe}$ or that is equal to L_{Rfe} if it is $\bar{L}_{Rfi}>L_{Rfe}$. In general it can be written:

$$V_{fi,\max}^{cf}\left(L_{Rfi}\right)=V_{fi,\max}^{bd}\left(L_{Rfi}\right) \tag{A11}$$

with:

$$L_{Rfi}=\begin{cases}\bar{L}_{Rfi} & if \quad \bar{L}_{Rfi}\le L_{Rfe}\\ L_{Rfe} & if \quad \bar{L}_{Rfi}>L_{Rfe}\end{cases} \tag{A12}$$

The expression $V_{fi,\max}^{cf}\left(L_{Rfi}\right)$ can be simplified, with respect to Eq. (16) of Bianco *et al.* 2011, by considering a concrete prism, relevant to the average available resisting bond length, that has its bases orthogonal to $\bar{L}_{Rfi}$, yielding:

$$V_{fi,\max}^{cf}\left(L_{Rfi}\right)=\min\left(L_{Rfi}\cdot\tan\alpha;\frac{b_w}{2}\right)\cdot\min\left(s_f\cdot\sin\beta;2\cdot L_{Rfi}\cdot\tan\alpha\right)\cdot f_{ctm} \tag{A13}$$

while the bond transferred force is given by Eq. (7.a) of Bianco et al. 2011, that is:

$$V_{fi,\max}^{bd}\left(L_{Rfi}\right)=L_p\cdot\frac{1}{J_1}\cdot\lambda\cdot\left\{C_1\cdot\left[\cos\left(\lambda\cdot L_{Rfi}\right)-1\right]-C_2\cdot\sin\left(\lambda\cdot L_{Rfi}\right)\right\} \tag{A14}$$

Substituting these latter into Eq. (A11), and taking into consideration the simplifications of Eq. (A9), one obtains:

$$f_{ctm}^{*}=\frac{L_p\cdot\lambda\cdot\delta_1\cdot\sin\left(\lambda\cdot L_{Rfi}\right)}{J_1\cdot\min\left(L_{Rfi}\cdot\tan\alpha;\frac{b_w}{2}\right)\cdot\min\left(s_f\cdot\sin\beta;2\cdot L_{Rfi}\cdot\tan\alpha\right)} \tag{A15}$$

With the simplifications of Eq. (A9), the value of imposed end slip in correspondence of which the bond-based constitutive law attains the peak, given by Eq. (13) of Bianco *et al.* 2011, simplifies into:

$$\delta_{L1}\left(\bar{L}_{Rfi}^{eq}\right)=\begin{cases}\delta_1\cdot\left[1-\cos\left(\lambda\cdot\bar{L}_{Rfi}^{eq}\right)\right] & \text{for } \bar{L}_{Rfi}^{eq}\le L_{Rfe}\\ \delta_1 & \text{for } \bar{L}_{Rfi}^{eq}>L_{Rfe}\end{cases} \tag{A16}$$

The expression of the maximum effective capacity $V_{fi,eff}^{\max} = V_{fi,eff}(\gamma_{\max})$, given by Eq. (20) of Bianco *et al.* 2011, can be further simplified, introducing the simplifications of Eqs. (A9) into:

$$V_{fi,eff}^{\max} = V_{fi,eff}(\gamma_{\max}) = \frac{\delta_1 \cdot A_2}{2 \cdot L_d \cdot A_3 \cdot \gamma_{\max}} \cdot \left[\frac{\pi}{2} - \arcsin\psi - \psi \cdot \sqrt{1-\psi^2} \right] \tag{A17}$$

in which

$$\psi = 1 - A_3 \cdot \gamma_{\max} \cdot L_d \tag{A18}$$

where A_3 and L_d were already introduced in the main text.